Monthly Notices
of the
ROYAL ASTRONOMICAL SOCIETY

Mon. Not. R. Astron. Soc. **424,** 779–788 (2012) doi:10.1111/j.1365-2966.2012.21265.x

Distinguishing between stellar and planetary companions with phase monitoring

Stephen R. Kane★ and Dawn M. Gelino

NASA Exoplanet Science Institute, Caltech, MS 100-22, 770 South Wilson Avenue, Pasadena, CA 91125, USA

Accepted 2012 May 8. Received 2012 May 8; in original form 2012 March 24

ABSTRACT

Exoplanets which are detected using the radial velocity technique have a well-known ambiguity of their true mass, caused by the unknown inclination of the planetary orbit with respect to the plane of the sky. Constraints on the inclination are aided by astrometric follow-up in rare cases or, in ideal situations, through subsequent detection of a planetary transit. As the predicted inclination decreases, the mass of the companion increases leading to a change in the predicted properties. Here we investigate the changes in the mass, radius and atmospheric properties as the inclination pushes the companion from the planetary into the brown dwarf and finally low-mass star regimes. We determine the resulting detectable photometric signatures in the predicted phase variation as the companion changes properties and becomes self-luminous. We apply this to the HD 114762 and HD 162020 systems for which the minimum masses of the known companions place them at the deuterium-burning limit.

Key words: techniques: photometric – brown dwarfs – stars: low-mass – planetary systems.

1 INTRODUCTION

Planets discovered using the radial velocity technique continue to form a major component of the known exoplanets. These planets have a well-known ambiguity to their masses due to the unknown inclination of their orbits. Some planets have subsequently been found to be more massive than originally thought when constraints are later placed upon their inclinations. These constraints can come from dynamical considerations, such as for the HD 10180 system (Lovis et al. 2011), through astrometric follow-up (Reffert & Quirrenbach 2011) or measurements of the projected equatorial velocity (Watson et al. 2010), although some hot Jupiters have been found to exhibit spin–orbit misalignment (see, for example, Winn et al. 2005). The consequence of these constraints can be either to confirm their planetary candidacy or to move the mass into the regime of brown dwarfs and low-mass stars.

The mass–radius relationship of short-period exoplanets is evolving through the discovery of numerous transiting exoplanets (Burrows et al. 2007; Fortney, Marley & Barnes 2007; Seager et al. 2007). The understanding of this relationship is undergoing continued and rapid evolution through the release of transiting planets from the Kepler mission (Borucki et al. 2011a,b). Surveys for transiting exoplanets have also led to the serendipitous discovery of transiting brown dwarfs, such as CoRoT-3b (Deleuil et al. 2008), WASP-30b (Anderson et al. 2011) and LHS6343C (Johnson et al. 2011). The mass–radius relationship of low-mass stars has been investigated by numerous authors (Ribas 2006; Demory et al. 2009; Fernandez et al. 2009; Kraus et al. 2011) through new radii measurements and the development of models to explain the observed relationship. Even so, the low-mass stars for which accurate radii have been determined remain a relatively small sample from which to draw upon to derive the theoretical framework for model construction. These mass–radii distributions give us clues about the formation mechanisms that occurred within these systems.

The phase functions and resulting photometric light curves of orbiting companions depend upon their radii and albedo as well as the orbital components (Seager, Whitney & Sasselov 2000; Sudarsky, Burrows & Hubeny 2005; Kane & Gelino 2010). Kane & Gelino (2011a) showed how the phase curves of exoplanets vary with inclination. However, it was assumed that the fundamental physical properties of the planet (such as mass, radius and atmospheric properties) remain the same. This is particularly relevant to planets discovered using the radial velocity technique since these planets are inherently subjected to an ambiguity in the mass with respect to the unknown orbital inclination. Here we expand upon this topic to investigate how the properties of a known companion can be expected to change as the inclination is decreased and therefore the mass is increased. If the companions are self-luminous, then this places an extra constraint upon what one can expect to see in high-precision observations designed to measure phase variations. We thus produce a criterion from which one can distinguish between stellar and planetary companions solely from high-precision photometric monitoring and without the need for astrometric observations.

★E-mail: skane@ipac.caltech.edu

© 2012 The Authors
Monthly Notices of the Royal Astronomical Society © 2012 RAS

Downloaded from http://mnras.oxfordjournals.org/ at California Institute of Technology on April 13, 2016

2 INCREASING THE COMPANION MASS

In this section, we describe the changing properties of a companion as the mass increases from the planetary regime, through the brown dwarf regime and into the realm of low-mass stars. We further investigate how these properties influence the photometric properties up to the self-luminous threshold.

2.1 Mass–radius dependence

The mass–radius relationship of exoplanets, brown dwarfs and low-mass stars is a difficult subject to relate to measurements since these require a system where the orbital inclination allows for the observations of eclipses and transits. Locating such systems involves the monitoring of many stars since the probability of having a favourable orbital inclination tends to be relatively low, depending upon the semi-major axis of the orbiting companion.

The radii for objects of a given mass depend upon a number of factors, including age and metallicity. Here we consider host stars which comprise the bulk of the known radial velocity hosts which have typical ages in the range 1–5 Gyr (Takeda et al. 2007). A study of 49 exoplanet host stars by Saffe, Gómez & Chavero (2005) found median ages of 5.2 and 7.4 Gyr, using chromospheric and isochrone methods, respectively, with dispersions of ∼4 Gyr. We thus consider objects which are of order 5 Gyr old.

The true mass of companions detected using the radial velocity technique is the measured mass divided by $\sin i$ where i is the orbital inclination relative to the plane of the sky. As the inclination decreases from an edge-on configuration ($i = 90^\circ$), the true mass increases which in turn affects the radius and atmospheric properties of the companion. It is generally held that the separation between planets and brown dwarfs is the onset of deuterium burning. However, the mass criteria for determining where deuterium burning occurs can be quite broad depending upon helium/deuterium abundances and metallicity (Spiegel, Burrows & Milsom 2011).

By way of demonstration, Fig. 1 plots the COND evolutionary model isochrones of Baraffe et al. (2003) for 1, 5 and 10 Gyr and for a mass range of 0.003–0.100 $M_\odot$. Also shown are the masses of two known exoplanets, HD 114762b (Latham et al. 1989) and HD 162020b (Udry et al. 2002). Assuming an inclination of $i = 90^\circ$, the measured mass of HD 114762b is $11.0 M_J$ (0.0105 $M_\odot$) whereas

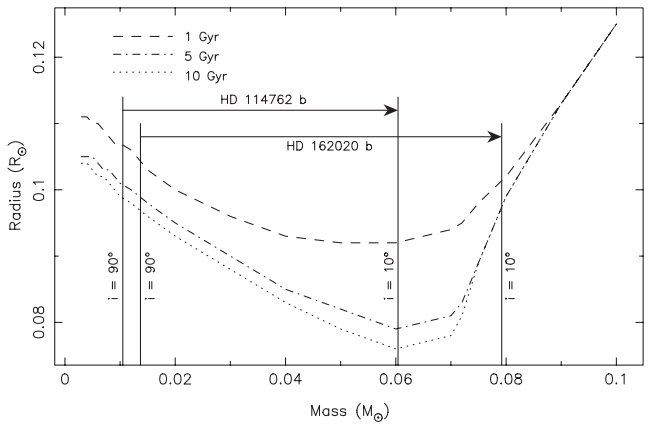

Figure 1. The mass–radius relationship of planets through to low-mass stars using the isochrones of Baraffe et al. (2003) for 1, 5 and 10 Gyr. The increasing masses of HD 114762b and HD 162020b are shown to demonstrate the effect of decreasing the inclination from an edge-on orbit ($i = 90^\circ$) to an almost face-on orbit ($i = 10^\circ$).

for a near face-on inclination of $i = 10^\circ$, the mass increases to $63.2 M_J$ (0.0604 $M_\odot$). According to the 5 Gyr isochrone, this reduces the predicted radius from 0.101 $R_\odot$ to 0.079 $R_\odot$. Kane et al. (2011) have excluded transits for this companion which thereby restricts the inclination to be less than 89°. For HD 162020b, the same change in inclination increases the measured mass of $14.4 M_J$ (0.0137 $M_\odot$) to $82.9 M_J$ (0.0792 $M_\odot$), thus decreasing the predicted radius from 0.099 $R_\odot$ to 0.097 $R_\odot$. In each case, the change in inclination moves them from the planetary regime to the brown dwarf/low-mass star boundary and beyond.

As noted in Section 1, our knowledge of companion radii in different mass regimes is a currently evolving topic. For example, an important consideration is the existence of the so-called brown dwarf desert (Grether & Lineweaver 2006; Kraus et al. 2008) which may bias inclinations away from this mass regime. The COND evolutionary models utilized above will undoubtedly undergo slight adjustments as the sample size of known low-mass transiting companions increases. One of the important parameters is the age of the host star. As shown in Fig. 1, the range of radii can be quite diverse for a given mass depending on which isochrone one adopts for the host star. However, the divergence is most significant for relatively young (∼1 Gyr) stars beyond which the radii converge upon a small range of radii for a large range of ages. Even so, one must consider the uncertainty in the host star age, assuming that the companion is of a similar age.

2.2 Impact on phase curves

For companions which are not self-luminous, there will be a photometric phase signature from the companion whose amplitude depends upon a variety of factors including the companions' radius, semi-major axis, eccentricity, orbital inclination and atmospheric properties (geometric albedo). Here we adopt the formalism of Kane & Gelino (2010, 2011a) to demonstrate the impact of the changing companion properties on phase curves.

The phase angle of the planet (α) is given by

$$\cos\alpha = \sin(\omega + f)\sin i, \tag{1}$$

where ω is the argument of periastron and f is the true anomaly. This angle is defined to be $\alpha = 0^\circ$ when the planet is on the opposite side of the star from the observer. Note that this means that $\cos\alpha = 1$ is only possible for edge-on orbits. All other inclinations will result in a more complicated dependence on the orbital parameters as described by Kane & Gelino (2011a).

The flux of a planet f_p and host star $f_\star$ has a ratio defined as

$$\epsilon(\alpha, \lambda) \equiv \frac{f_\mathrm{p}(\alpha, \lambda)}{f_\star(\lambda)} = A_\mathrm{g}(\lambda) g(\alpha, \lambda) \frac{R_\mathrm{p}^2}{r^2}, \tag{2}$$

where the flux is measured at wavelength λ, $A_\mathrm{g}(\lambda)$ is the geometric albedo, $g(\alpha, \lambda)$ is the phase function and R_p is the radius of the planet. The star–planet separation r is given by

$$r = \frac{a(1 - e^2)}{1 + e\cos f}, \tag{3}$$

where a is the semi-major axis and e is the orbital eccentricity. The phase function is primarily dependent upon the phase angle, whether one assumes a Lambert sphere or something more complicated to describe the scattering properties. The geometric albedo for gas giant planets depends upon the incident flux (star–planet separation) since this can determine the amount of reflective condensates that can maintain a presence in the upper atmospheres (Sudarsky et al. 2005; Kane & Gelino 2010).

Downloaded from http://mnras.oxfordjournals.org/ at California Institute of Technology on April 13, 2016

A component of equation (2) which explicitly relies upon the companion properties is the radius squared. As shown in Section 2.1, variation of the companion mass in the range 0.003–0.100 $M_\odot$ can vary the radius by as much as ∼20 per cent. This results in a variation of the flux ratio amplitude by as much as ∼40 per cent. The uncertainty in both the planetary radius and albedo is discussed further in Section 6. For now, we note that there is an apparent degeneracy in the predicted radius as a function of mass in the isochrones shown in Fig. 1 due to the minimum located at 0.06 $R_\odot$. However, beyond this value, the companions start to become self-luminous. This is discussed in further detail in Section 3.

2.3 Ellipsoidal variations

An additional possible effect of an increased mass is the induction of ellipsoidal variations in the host star. Drake (2003) has proposed the use of ellipsoidal variations as a tool in eliminating false positives due to eclipsing binaries from transit surveys. Stellar ellipsoidal variations have been previously detected for short-period giant planet systems though, such as the case of HAT-P-7b which was observed to have signatures of phase as well as ellipsoidal variations in Kepler data (Welsh et al. 2010). The detection of ellipsoidal variations in the context of the Kepler mission is discussed in detail by Pfahl, Arras & Paxton (2008).

Comparison of phase and ellipsoidal variation amplitudes to those induced by reflex Doppler motion has been undertaken in several studies, including those by Loeb & Gaudi (2003) and Zucker, Mazeh & Alexander (2007). A full expansion of the discrete Fourier series for the ellipsoidal variation amplitude is provided by Morris & Naftilan (1993). Here we adopt the approximate relation used by Loeb & Gaudi (2003) as follows:

$$\frac{\Delta F}{F_0} \sim \beta \frac{M_\mathrm{p}}{M_\star} \left(\frac{R_\star}{a} \right)^3, \tag{4}$$

where β is the gravity-darkening exponent. For the purposes of demonstration, we have assumed $\beta = 0.32$ as determined by Lucy (1967). We refer the reader to Claret (2000) for a much more thorough treatment of the dependence of β on various stellar properties. Fig. 2 shows how the ellipsoidal variation amplitude can be expected to change as a function of companion mass for three different orbital periods. The scale used on the x axis is identical to that in Fig. 1. As one would expect from equation (4), a change in the companion mass results in an almost linear change in the observed flux ratio changes ('almost' since changing the mass also changes the semi-major axis at which the expected period occurs). Changing the period has a much more dramatic effect. Note however that a low-mass star in a 10 d orbit will induce a similar ellipsoidal variation to a giant planet in a 5 d orbit.

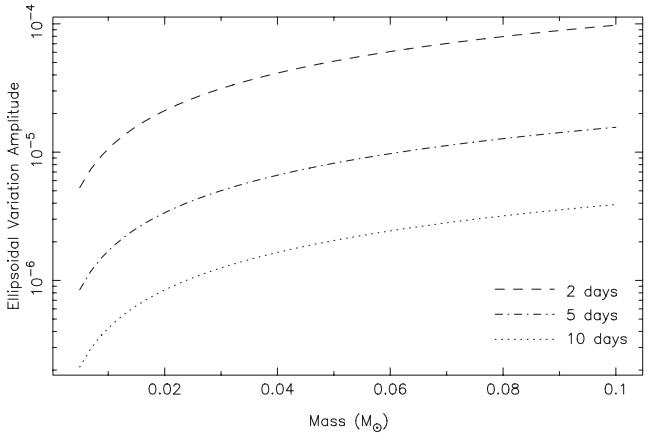

Figure 2. The mass dependence of the predicted ellipsoidal variation amplitude and the same range of masses as shown in Fig. 1 for three different periods.

There are numerous examples of a changing tidal distortion amplitude due to eccentric orbits, such as those contained in Soszyński et al. (2004). To account for orbital eccentricity and inclination, we modify equation (4) as follows:

$$\frac{\Delta F}{F_0} \sim \beta \frac{M_\mathrm{p}}{M_\star} \left(\frac{R_\star}{r} \right)^3 \left(\cos^2(\omega + f) + \sin^2(\omega + f) \cos^2 i \right)^{\frac{1}{2}}, \tag{5}$$

where we have replaced a with r, as per equation (3). If there is significant orbital eccentricity present, one can use this as an additional diagnostic in interpreting the uniqueness of the ellipsoidal variation solution. However, eccentric orbits are far more likely to occur at longer periods where the amplitude of the variation is greatly reduced.

3 CROSSING THE SELF-LUMINOUS THRESHOLD

Moving from the brown dwarf into the low-mass star regime introduces many changes associated with the companion becoming self-luminous. Planets and brown dwarfs are typically not self-luminous except at a young age (<1 Gyr). For brown dwarfs engaged in deuterium burning, the transition to hydrogen burning will abort if the mass is less than ∼0.07 $M_\odot$ after which the object will undergo luminosity decay beyond an age of ∼1 Gyr. A full description of object characteristics in terms of age, helium/deuterium fraction and metallicity can be found in Burrows et al. (1993). Here we briefly discuss the main features that one can expect to observe as the object crosses the self-luminous threshold.

3.1 Elimination of the phase function

A major feature of planetary phase functions is that it relies on reflected light which is incident from the host star. If the dominant source of light from the companion becomes that which originates from self-luminosity, then there will no longer be a phase function of the kind described earlier. To account for this, we include a gradual decrease in the phase variation amplitude for companion masses $>50 M_J$. There will however be an increasing likelihood of observable ellipsoidal variations with increasing mass (see Section 2.3) such that these variations may subsume the decreasing phase effects.

An additional effect which may produce a phase-like signature is the 'reflection effect', a well-known phenomenon for close binary stars in which the irradiation of one component by the other results in a differential flux over the irradiated star surface (Wilson 1990). Application of this process to binary systems consisting of a star and a giant planet or brown dwarf is considered by Budaj (2011), although Green et al. (2003) argue that this heating of the primary star due to the presence of even a close-in gas giant planet will be negligibly small. The irradiation will only become comparable to the amplitude of the phase variation when the mass enters the low-mass star regime, at which point the convective atmosphere will in turn have an increased albedo due to irradiation from the primary (Harrison et al. 2003).

For planetary and brown dwarf companions, the heating of the day-side may result in significant thermal flux being re-radiated.

Downloaded from http://mnras.oxfordjournals.org/ at California Institute of Technology on April 13, 2016

This depends not only on the incident flux but also on the fundamental atmospheric properties which govern radiative and advective time-scales (Fortney et al. 2008; Showman et al. 2009; Kane & Gelino 2011b). Thus, efficient atmospheric re-circulation of the received heat to the night side of the planet may be sufficient to suppress an overall phase function at infrared wavelengths.

3.2 Introduction of stellar activity

At the level of photometric precision required here, it is important to consider the level of intrinsic stellar variability. Depending upon the properties of the companion, there may be intrinsic stellar activity which reveals its nature through precision photometry. There are now hundreds of known brown dwarfs with an increasing understanding of their atmospheres and activity (Kirkpatrick et al. 2011). However, activity and rotation rates amongst brown dwarfs and low-mass stars can vary greatly, mostly due to the large range of temperatures and ages of those objects monitored. Surveys of relatively young low-mass stars tend to show signs of high chromospheric magnetic activity and increased rotation rates with decreasing temperature (Jenkins et al. 2009; Becker et al. 2011; Scholz et al. 2011). A spectral analysis of an M dwarf sample by Browning et al. (2010) showed that increased rotation appears to be more common in stars later than M3, indicating that measurable rotational braking is reduced for fully convective stars. Berta et al. (2011) investigated the variability of the exoplanet hosting star GJ 1214 ($0.16\,M_{\odot}$) and found a periodicity of 53 d with an amplitude of 3.5 millimags at the MEarth bandpass. Clearly if one has the precision to detect planetary phase variations, then one also has the capability to detect stellar activity from the companion. Indeed it is expected that a low-mass star instead of planetary companion will show larger chromospheric and coronal activity compared with equivalent single stars (Zaqarashvili, Javakhishvili & Belvedere 2002). If the orbital parameters of the companion are sufficiently understood from radial velocity measurements, then one can extract the variability signals of the companion and the host star. There may be cases where the orbital period of the companion is close to the rotation period of the star, which is generally in the range of 10–40 d for radial velocity host stars (Simpson et al. 2010). In such cases, the peaks in the power spectrum from a Fourier analysis of the photometry may separate to a degree where starspot variability due to rotation can be isolated.

This discussion is referring to the activity of a potential stellar-mass companion. However, the intrinsic stellar variability could well be substantially stronger than these effects. An analysis of Kepler data by Ciardi et al. (2011) found that most dwarf stars are stable down to the precision of the Kepler spacecraft, with G-dwarfs being the most stable of the studied spectral types. The main cause of photometric variability in F–G–K stars is starspots and rotation, as verified by the Kepler variability study performed by Basri et al. (2011). Since the orbital period of the radial velocity target stars is well determined, this will aid in separating the signals of planetary phase from that of the host star variability whose period is likely related to the stellar rotation period. It should be noted that disentangling the variability of the host star may result in an increase in the observing time requirement.

3.3 Doppler boosting

Doppler boosting occurs due to a relativistic effect which creates an apparent increase and decrease in the light from the host star when it is moving towards and away from the observer. The fractional amplitude of the effect is given by

$$\frac{\Delta F}{F_0} = \frac{(3-\alpha)K}{c}, \tag{6}$$

where K is the radial velocity semi-amplitude and α is the derivative of the bolometric flux with respect to the frequency in the stationary frame of reference. This effect has been discussed in terms of planetary companions and high-precision photometry by Loeb & Gaudi (2003) and Faigler & Mazeh (2011). Doppler boosting due to stellar-mass companions has been detected in the photometry from the Kepler mission (van Kerkwijk et al. 2010; Faigler et al. 2012). The photometric variability, including Doppler boosting, induced by KOI-13.01 led to its confirmation as a planet (Shporer et al. 2011; Mazeh et al. 2012). It was additionally shown by Loeb & Gaudi (2003) and Shporer et al. (2011) that the effect of Doppler boosting can be significantly larger than those from phase and ellipsoidal variations for orbital periods greater than $\sim$10 d.

We consider planets which have been detected with precision radial velocities. The amplitude of Doppler boosting is directly proportional to K and thus we remove this effect with only one free parameter. Note that observing this effect does not remove the $\sin i$ ambiguity of the companion mass. This is discussed further in Section 4.

3.4 The O'Connell effect

The O'Connell effect refers to the height difference that may occur between the maxima in the light curves of close binary stars. There are several possible causes for this effect, such as starspots or gas streaming between the binary components. This effect has been previously studied for eclipsing binary stars by Davidge & Milone (1984) and more recently by Wilsey & Beaky (2009). Binaries with low-mass stellar companions are known to exhibit this effect (Austin et al. 2007), making this a noteworthy phenomenon here. In particular, the precision of data from the Kepler mission allows an unprecedented investigation of the frequency and source of this effect.

In Fig. 3 we show two example light curves which show several of the effects discussed in this section, Kepler IDs 8386198 and 9544350. These data are corrected flux values from the Quarter 2 release of the Kepler mission, extracted using the Kepler interface of the NASA Exoplanet Archive.[1] These stars were included in the Kepler Eclipsing Binary Catalog[2] by Prsa et al. (2011) as having signatures due to ellipsoidal variations but they can also be seen to have clear O'Connell effect signatures. The amplitudes of these variations are substantial: 5–10 millimags, and so are well within detection thresholds for stellar-mass companions (see Fig. 2). This is also significantly larger than the previously mentioned variations and so care must be taken to distinguish this effect from those more subtle in amplitude.

4 OBSERVABLE SIGNATURES

Here we combine the effects we have considered in previous sections and apply them to the two examples discussed earlier, HD 114762b and HD 162020b. Recall that these various observable signatures are being considered for companions which are known through their precision radial velocity detections. In the case of the

[1] http://exoplanetarchive.ipac.caltech.edu/
[2] http://astro4.ast.villanova.edu/aprsa/kepler/

Downloaded from http://mnras.oxfordjournals.org/ at California Institute of Technology on April 13, 2016

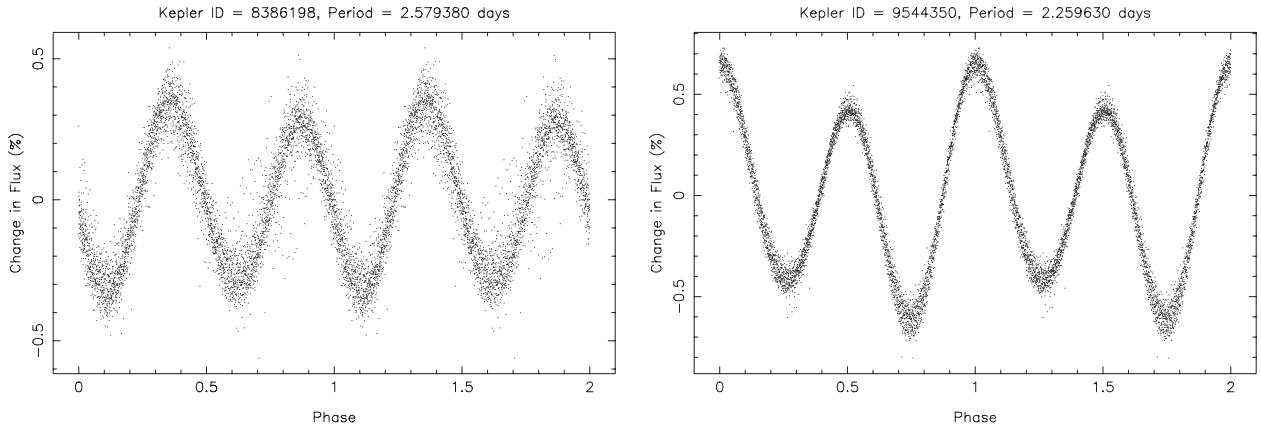

Figure 3. Light curves from Quarter 2 Kepler data for two cases of ellipsoidal variations, Kepler IDs 8386198 (left panel) and 9544350 (right panel). The fluxes have been converted to percentage variations against the mean flux of the data.

two examples being considered here, the radial velocity amplitudes are 612 and 1813 m s^{-1} which lead to fractional Doppler boosting amplitudes of 8.8×10^{-6} and 2.6×10^{-5}, respectively. For the orbits of these planets, we assume that Doppler boosting effects may be well characterized and we inject the two remaining and comparable effects of ellipsoidal and phase variations.

It was shown by Kane & Gelino (2011a) that the phase signature one expects from a planet in an eccentric orbit is intricately related to both the inclination and periastron argument of the orbit. If one also includes the companion mass, radius and various other photometric signatures as free parameters, then it can become difficult to disentangle the physical model to account for the observations. Shown in Fig. 4 is an example sequence of photometric signatures from a simulated companion in a 5 d orbit around a solar-type star. The companion has a minimum mass of $M_p \sin i = 10 M_J$ and is in an eccentric orbit ($e = 0.2$) where periastron passage occurs between the observer and the star ($\omega = 90^\circ$). In each panel, the dashed line is the phase variation, the dotted line is the ellipsoidal variation and the solid line is the total combined signature. The flux ratio refers to the apparent change in flux of the host star, either by reflected light by the companion or the ellipsoidal distortion of the stellar shape. An orbital phase of zero corresponds to when the companion is at superior conjunction. Thus, the phase variation tends to peak near phase zero whereas (for edge-on orbits, depicted in the top panel) the ellipsoidal variation has two minima: when the companion is either behind or in front of the star. At this inclination, the companion is considered to be of planetary mass and the phase signature dominated the photometric variability. The middle panel shows the effect of reducing the inclination to 30° such that the mass of the companion has now doubled. The phase amplitude is now much reduced and the ellipsoidal distortion of the star as the companion passes through periastron passage is more visible. At an inclination of 10° (shown in the bottom panel), the orbit is now observed almost face-on. The companion is a high-mass brown dwarf and the phase signature is almost eliminated, partly due to the slightly reduced size but mostly due to the reduced contrast between the day and night side of the companion as it becomes more self-luminous. Note also the greatly increased amplitude of the ellipsoidal variations.

4.1 HD 114762b

Shown in Fig. 5 are the predicted photometric variations expected for the companion orbiting HD 114762. We use the stellar and orbital parameters measured by Kane et al. (2011). This companion has a minimum mass of $M_p \sin i = 10.98 \pm 0.09 M_J$ and is in an ∼84 d period orbit with an eccentricity of 0.34. The periastron argument of $\omega = 201\overset{\circ}{.}28$ means that periastron passage takes place almost behind the star where the orbital phase is ∼0.95. Recall from equations (2) and (5) that phase and ellipsoidal variations are proportional to r^{-2} and r^{-3}, respectively. Thus in this case, the phase variations dominate the signature until the mass is pushed high into the brown dwarf regime as shown in the bottom panel.

There are several aspects of note here. Due to the relatively large star–planet separation, there is only a small change in the total flux. However, as the phase signature disappears and the ellipsoidal signature grows, the total flux stays approximately the same. Note that there is a phase offset between the peak of ellipsoidal and phase variations. The peak of the ellipsoidal variation depends on the star–planet separation and the orientation of the major axis of the distorted stellar profile, whereas the phase variation also depends upon the phase function of the planet. This is the key which unlocks the difference between the planetary and stellar companion signatures in this case since one can detect the change in phase far more easily than one can detect the change in amplitude of the signature.

4.2 HD 162020b

Fig. 6 shows the equivalent predicted photometric variations for the companion to HD 162020. The minimum mass is $M_p \sin i = 14.4 M_J$ and the orbital period and eccentricity are 8.43 d and 0.277, respectively, with a periastron argument of $\omega = 28\overset{\circ}{.}4$. These orbital parameters are from the measurements of Udry et al. (2002), who estimate the host star as being K3V. We derive a radius for the host star by applying the surface gravity $\log g$ from Valenti & Fischer (2005) to the relation

$$\log g = \log\left(\frac{M_\star}{\mathrm{M}_\odot}\right) - 2\log\left(\frac{R_\star}{\mathrm{R}_\odot}\right) + \log g_\odot, \quad (7)$$

where $\log g_\odot = 4.4374$ (Smalley 2005). From this we calculate a stellar radius of $R_\star = 0.52\,\mathrm{R}_\odot$. We additionally calculate the radius using the relations of Torres, Andersen & Giménez (2010) and find $R_\star = 0.53 \pm 0.03\,\mathrm{R}_\odot$. The ellipsoidal variations are sensitive to the radius of the host star (see equation 5) but the consistency of the radius determinations and

Downloaded from http://mnras.oxfordjournals.org/ at California Institute of Technology on April 13, 2016

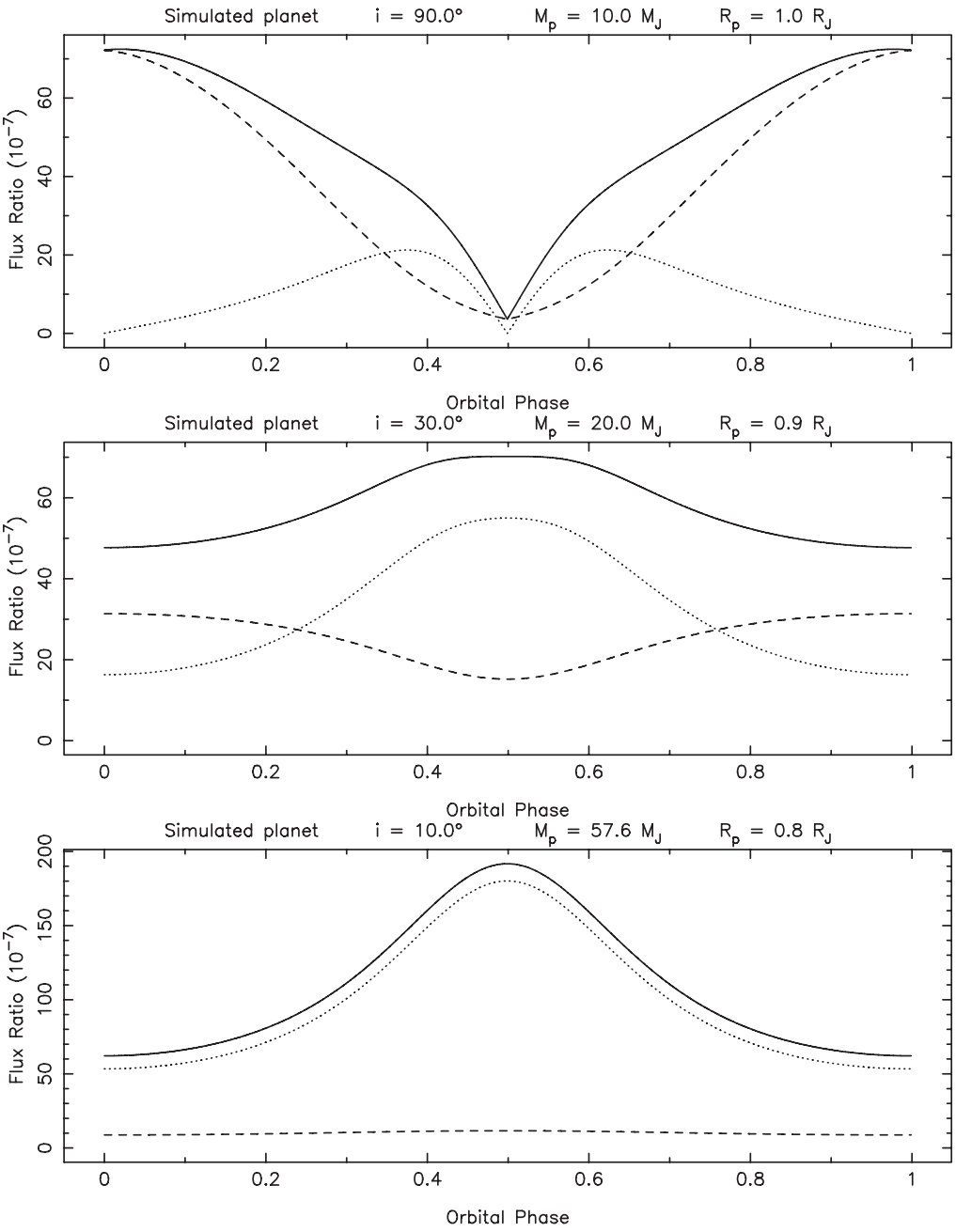

Figure 4. Photometric signature for a simulated companion in a 5 d eccentric ($e = 0.2$, $\omega = 90^\circ$) orbit around a solar-type star. An orbital phase of zero corresponds to when the companion is at superior conjunction. The dashed line is the phase variation, the dotted line is the ellipsoidal variation and the solid line is the total combined signature. The three panels show the effect of changing the inclination of the system from edge-on ($i = 90^\circ$, top panel) to the smaller inclinations shown in the bottom two panels.

small uncertainties means that the calculated amplitude is quite robust.

The panels of the figure show that the phase variations are able to dominate the total signature even when the inclination is decreased to 30°. However, as the mass rapidly increases beyond this point, the phase variations drop to zero. By the time an inclination of 10° is reached, it is clear that the companion is able to sustain hydrogen burning and the photometric variations and now due to tidal distortions induced by the eccentric orbit. As was the case with HD 114762b, the total amplitude of the variations does not significantly change but the phase offset grows as the ellipsoidal variations emerge as the dominant effect.

5 A NOTE ON SPECTRAL LINE DETECTION

An additional effect of increasing the companion mass is the introduction of absorption bands which are characteristic of brown dwarfs and late-type stars. One may then wonder if such features would become apparent in high-precision spectral data or if the companion and its star could be considered a spectroscopic binary. The optical spectrum of an M dwarf is typically dominated by TiO and VO absorption bands. Considerable progress has been made on characterizing the properties of the cooler L dwarfs. An example of an L dwarf was detected using both radial velocities and high-resolution imaging orbiting the solar analog HR 7672 by Liu et al.

Downloaded from http://mnras.oxfordjournals.org/ at California Institute of Technology on April 13, 2016

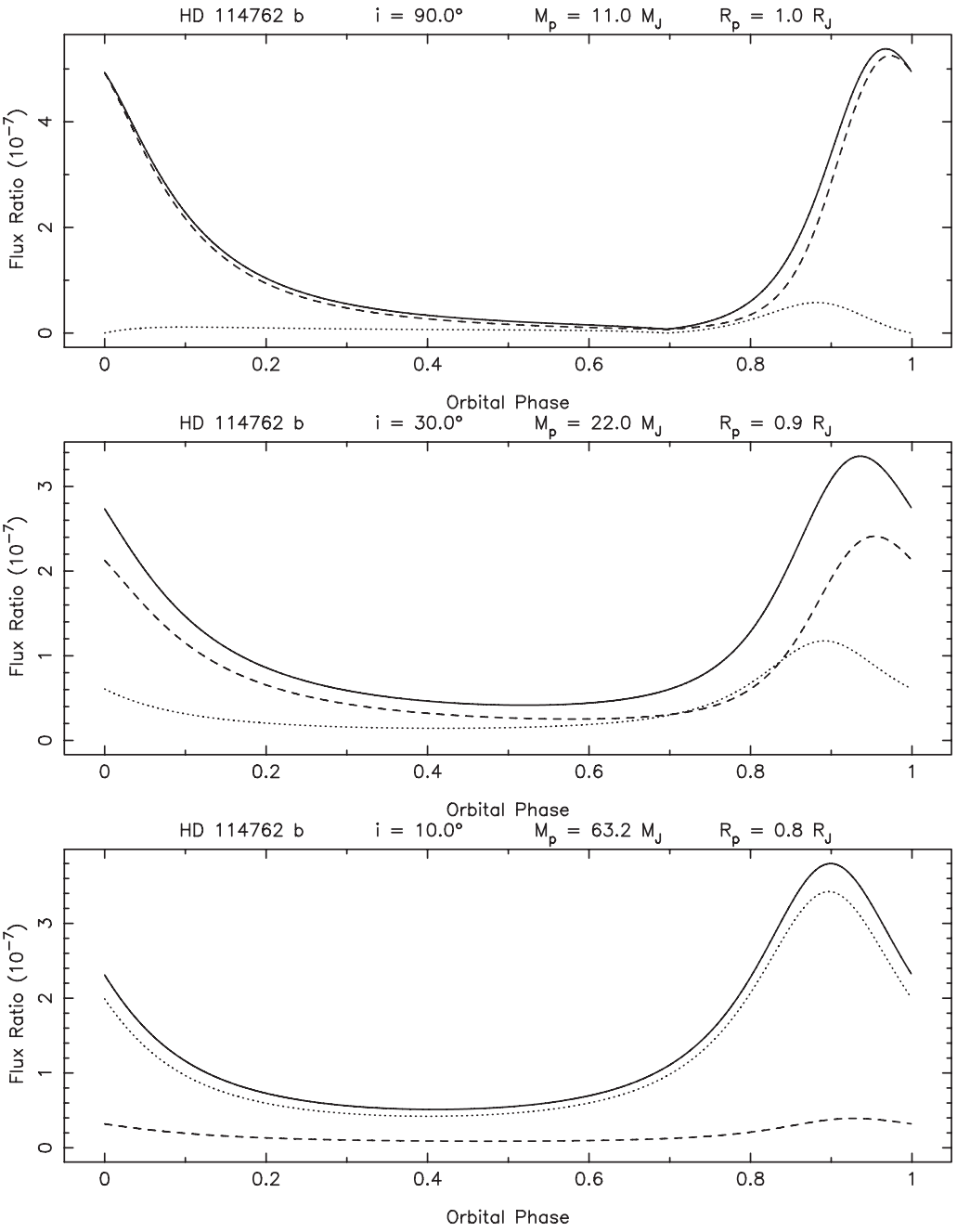

Figure 5. Predicted photometric signatures for the companion to HD 114762. The dashed line is the phase variation, the dotted line is the ellipsoidal variation and the solid line is the total combined signature. The three panels show the effect of changing the inclination of the system from edge-on ($i = 90^\circ$, top panel) to the smaller inclinations shown in the bottom two panels.

(2002). The L dwarf prototype, GD 165B, has been used to model the spectra of many similar types of brown dwarfs through the identification of prominent spectral features (Kirkpatrick et al. 1999). In particular, L dwarfs exhibit strong metal hydride bands and alkali metal lines. Kirkpatrick et al. (1999) found the Na doublet at 8183, 8195 Å to be especially strong and a possible candidate for detection in optical passbands. For the even cooler T dwarfs, such as Gl 229B, the methane absorption bands and broad absorption features due to alkali metals tend to dominate near-infrared (NIR) spectra (Saumon et al. 2000; Sengupta & Krishan 2000). The major hinderance facing detection prospects for these features is that they primarily manifest at red wavelengths where the flux is dramatically reduced at optical passbands. Thus, resolution of the companion properties through spectral line detection is better suited to the NIR instruments which are being developed to perform searches for exoplanets around late-type stars.

6 THE UNKNOWN RADIUS AND ALBEDO

A major source of uncertainty in the discussion thus far results from the radius and albedo of the planet. These are generally unknown for non-transiting planets and so we are using models to describe their dependence on the other measured properties, such as mass. Equation (2) shows that the planet-to-star flux ratio depends linearly

© 2012 The Authors, MNRAS **424,** 779–788
Monthly Notices of the Royal Astronomical Society © 2012 RAS

Downloaded from http://mnras.oxfordjournals.org/ at California Institute of Technology on April 13, 2016

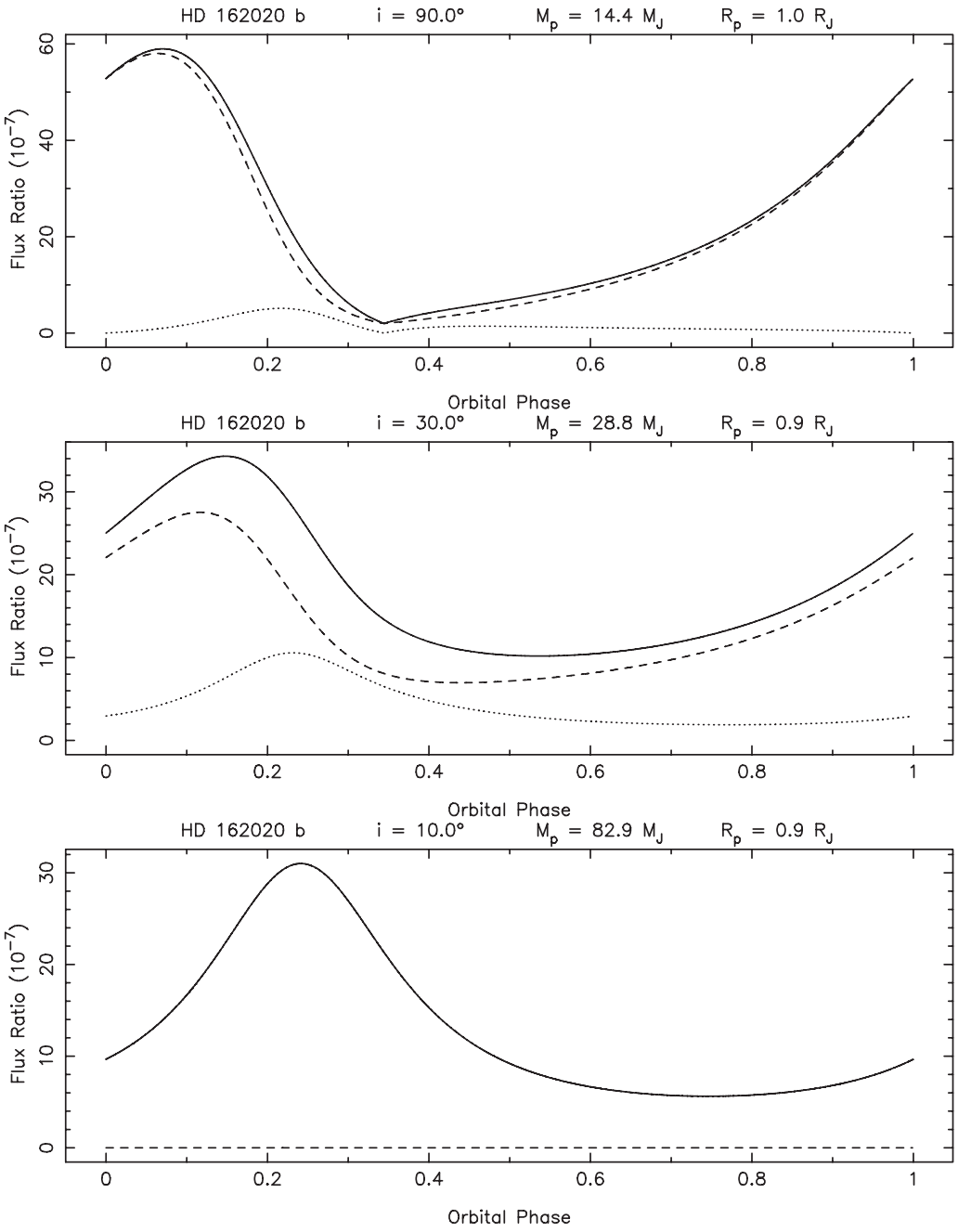

Figure 6. Predicted photometric signatures for the companion to HD 162020. The dashed line is the phase variation, the dotted line is the ellipsoidal variation and the solid line is the total combined signature. The three panels show the effect of changing the inclination of the system from edge-on ($i = 90^\circ$, top panel) to the smaller inclinations shown in the bottom two panels.

on the albedo and quadratically on the planetary radius. Conversely, these planetary properties have no impact on either the ellipsoidal or Doppler boosting variations. The simulations shown in Section 4 demonstrate that the contribution of the planetary phase to the total variations becomes significantly less when the orbit is close to face-on, even for eccentric orbits. Thus, the uncertainties in the radius and albedo become particularly important for one to be able to discern the planetary properties for low inclination orbits.

Regarding planetary albedo, there has been considerable effort to produce analytic models for estimating the albedo at a given star–planet separation, such as the work of Cahoy, Marley & Fortney (2010), Madhusudhan & Burrows (2012) and Selsis, Wordsworth & Forget (2011). The situation is more complicated than a simple distance–albedo relation however, as shown by the recent discovery of a surprisingly high albedo for Kepler-7b (Demory et al. 2011). Cowan et al. (2012) provide a summary of the recent geometric albedo measurements, the diversity of which may partially be a function of the heat redistribution efficiency in the high equilibrium temperature regime. Demory et al. (2011) attribute the anomalously high albedo of Kepler-7b as being due to a combination of Rayleigh scattering and clouds. It is also possible that a smooth dependence of albedo on star–planet separation is broken by phase transitions whereby removed reflective condensates reappear in the upper atmosphere as clouds for a small range of equilibrium temperatures,

Downloaded from http://mnras.oxfordjournals.org/ at California Institute of Technology on April 13, 2016

thus increasing the albedo. Clearly we require a greater understanding of giant planet albedos in order to be able to unambiguously extract the phase variation component for non-transiting planets.

Regarding planetary radius, our understanding of the mass–radius relationship is developing rapidly as pointed out in Section 1. Based upon the current knowledge of transiting planets, Kane & Gelino (2012) show that the radii of planets with masses greater than $\sim$0.3 Jupiter masses follow an approximately linear model. This mass range also encompasses the majority of non-transiting planets for which their planetary status is ambiguous. It is expected that the variation seen within this region is due in no small part to the fact that highly irradiated giant planets dominate this sample due to the bias of the transit technique. However, Kepler is improving our understanding of planetary radii at a larger range of period than that which is encompassed by the ground-based surveys. The proposed Transiting Exoplanet Survey Satellite (TESS) will not only add to this understanding but will also benefit from the follow-up potential of the planet discoveries due to the brightness of the host stars (Ricker et al. 2010).

Ultimately the results here rely upon the not unreasonable expectation that our knowledge of planetary radii and atmospheres will improve dramatically in future years. The combination of this improved knowledge and the availability of precision photometry will aid greatly towards breaking the degeneracy in these models.

7 FEASIBILITY DISCUSSION

The models presented here show that changing the mass of the companion will result in unique signatures which can be used to constrain the mass and subsequent properties of the companion. Such a detection of these signatures presents a significant challenge to instrumentation requirements and our current understanding of the mass–radius relationship. The precision requirement for successful detection of the signatures for the two examples provided is photometry with an accuracy of $\sim 10^{-7}$. The photometer for the Kepler mission is designed to achieve high-precision photometry over the 6.5 h window of a transit, but is not designed for long-term stability over the lifetime of the mission (Borucki et al. 2010). The orbits of the radial velocity planets are well understood in most cases and so we can accurately predict both the amplitude of the predicted phase signature and also the phase and times of maximum and minimum flux ratios. In contrast, the vast majority of Kepler targets are too faint for the acquisition of accurate radial velocity measurements and so predicting these times for eccentric orbits amongst Kepler targets is more difficult. The aforementioned TESS mission will provide an opportunity to perform high precision photometry on these bright host stars, many of which will have known radial velocity planets. The expectation that TESS will have sufficient photometric precision to detect down to Earth-mass planets around F–G–K stars means that this will be very close to the precision requirements for this experiment. The planned Lyot coronagraph on NIRCam for the James Webb Space Telescope may be able to achieve phase detections for a sample of the most favourable targets though in this case the instrument is optimized towards young planets around late-type stars.

Ground-based observations face more challenges in terms of correcting for atmospheric stability. However, future generation telescopes will provide opportunities to achieve very high precision, such as the European Extremely Large Telescope, the Thirty Metre Telescope and the Giant Magellan Telescope. One example of how high precision can be achieved from such telescopes has been provided by Colón et al. (2010) whose use of tunable narrow-band filters with the Gran Telescopio Canarias enabled a photometric precision of <0.05 per cent. Further developments of custom filters, adaptive optics systems and next-generation telescopes will hopefully provide a competitive ground-based source for achieving high photometric precision.

A possible alternative approach to detecting the inclination is astrometric follow-up of these targets, such as that carried out using *Hipparcos* data by Reffert & Quirrenbach (2011). The amplitude of the astrometric signal is roughly proportional to the mass of the secondary component. We refer the reader to Kane (2011) for a more concise comparison of exoplanet detection methods in the long-period regime. Thus, the examples shown in Section 2.1 will lead to a factor of $\sim$5 increase in the expected astrometric signal. This still results in astrometric signals at the μarcsec level and a challenge to detect from the ground. However, the space-based Gaia mission is predicted to have a single-measurement astrometric precision of 5–5.5 μarcsec (Casertano et al. 2008) and will therefore contribute greatly to sifting high-mass companions from the current exoplanet sample (Sozzetti et al. 2001).

8 CONCLUSIONS

Perhaps the main ambiguity that is inherent to detections of radial velocity exoplanets is the inclination of the orbit which produces a measurement of the minimum mass rather than the mass itself. The methods described here primarily rely on the physical properties of the companion to distinguish between various classes of orbits, as opposed to using the orbital properties as proposed by Black (1997). The different classes of objects which lie along the mass spectrum from planets to low-mass stars are becoming better understood in terms of their atmospheres and photospheric activity. However, the change in mass alone is enough to produce distinct signatures which can distinguish planets from higher mass objects.

In practice, detection of these signatures is going to be difficult to accomplish, even if one can achieve the needed precision. Once the mass increases to the point where hydrogen burning can be sustained, the variability effects are numerous leading to a veritable plethora of possible phase curves for the combined system. Note, for example, that we have not considered the changing gravity darkening of the host star due to a variable star–planet distance. The required precision is becoming achievable however with current and planned space-based observing platforms. Note that even though the data from the Kepler mission is an excellent example of such exquisite precision, the mission is searching for transits of objects around relatively faint stars (Borucki et al. 2010). Hence, these targets tend to have small prospects for a radial velocity orbital solution and no ambiguity with regard to their inclination. The kind of post-discovery analysis suggested here is therefore more suitable towards missions which can easily target the bright stars that comprise the bulk of radial velocity exoplanet host stars. Missions such as TESS will be able to monitor such stars as well as conducting the survey for new transiting systems (Deming et al. 2009).

ACKNOWLEDGMENTS

The authors would like to thank Davy Kirkpatrick, John Stauffer, David Ciardi and William Welsh for several useful discussions. We would also like to thank the anonymous referee whose comments greatly improved the quality of the paper. This research has made use of the NASA Exoplanet Database, which is operated by the Jet Propulsion Laboratory, California Institute of Technology, under contract with the National Aeronautics and Space Administration.

Downloaded from http://mnras.oxfordjournals.org/ at California Institute of Technology on April 13, 2016

REFERENCES

Anderson D. R. et al., 2011, ApJ, 726, L19
Austin S. J., Robertson J. W., Tycner C., Campbell T., Honeycutt R. K., 2007, ApJ, 133, 1934
Baraffe I., Chabrier G., Barman T. S., Allard F., Hauschildt P. H., 2003, A&A, 402, 701
Basri G. et al., 2011, AJ, 141, 20
Becker A. C., Bochanski J. J., Hawley S. L., Ivezić Z., Kowalski A. F., Sesar B., West A. A., 2011, ApJ, 731, 17
Berta Z. K., Charbonneau D., Bean J., Irwin J., Burke C. J., Désert J.-M., Nutzman P., Falco E. E., 2011, ApJ, 736, 12
Black D. C., 1997, ApJ, 490, L171
Borucki W. J. et al., 2010, Sci, 327, 977
Borucki W. J. et al., 2011a, ApJ, 728, 117
Borucki W. J. et al., 2011b, ApJ, 736, 19
Browning M. K., Basri G., Marcy G. W., West A. A., Zhang J., 2010, ApJ, 139, 504
Budaj J., 2011, AJ, 141, 59
Burrows A., Hubbard W. B., Saumon D., Lunine J. I., 1993, ApJ, 406, 158
Burrows A., Hubeny I., Budaj J., Hubbard W. B., 2007, ApJ, 661, 502
Cahoy K. L., Marley M. S., Fortney J. J., 2010, ApJ, 724, 189
Casertano S. et al., 2008, A&A, 482, 699
Ciardi D. R., von Braun K., Bryden G., van Eyken J., Howell S. B., Kane S. R., Plavchan P., Stauffer J. R., 2011, AJ, 141, 108
Claret A., 2000, A&A, 363, 1081
Colón K. D., Ford E. B., Lee B., Mahadevan S., Blake C. H., 2010, MNRAS, 408, 1494
Cowan N. B., Machalek P., Croll B., Shekhtman L. M., Burrows A., Deming D., Greene T., Hora J. L., 2012, ApJ, 747, 82
Davidge T. J., Milone E. F., 1984, ApJS, 55, 571
Deleuil M. et al., 2008, A&A, 491, 889
Deming D. et al., 2009, PASP, 121, 952
Demory B.-O. et al., 2009, A&A, 505, 205
Demory B.-O. et al., 2011, ApJ, 735, L12
Drake A. J., 2003, ApJ, 589, 1020
Faigler S., Mazeh T., 2011, MNRAS, 415, 3921
Faigler S., Mazeh T., Quinn S. N., Latham D. W., Tal-Or L., 2012, ApJ, 746, 185
Fernandez J. M. et al., 2009, ApJ, 701, 764
Fortney J. J., Marley M. S., Barnes J. W., 2007, ApJ, 659, 1661
Fortney J. J., Lodders K., Marley M. S., Freedman R. S., 2008, ApJ, 678, 1419
Green D., Matthews J., Seager S., Kuschnig R., 2003, ApJ, 597, 590
Grether D., Lineweaver C. H., 2006, ApJ, 640, 1051
Harrison T. E., Howell S. B., Huber M. E., Osborne H. L., Holtzman J. A., Cash J. L., Gelino D. M., 2003, ApJ, 125, 2609
Jenkins J. S., Ramsey L. W., Jones H. R. A., Pavlenko Y., Gallardo J., Barnes J. R., Pinfield D. J., 2009, ApJ, 704, 975
Johnson J. A. et al., 2011, ApJ, 730, 79
Kane S. R., 2011, Icarus, 214, 327
Kane S. R., Gelino D. M., 2010, ApJ, 724, 818
Kane S. R., Gelino D. M., 2011a, ApJ, 729, 74
Kane S. R., Gelino D. M., 2011b, ApJ, 741, 52
Kane S. R., Gelino D. M., 2012, PASP, 124, 323
Kane S. R. et al., 2011, ApJ, 735, L41
Kirkpatrick J. D., Allard F., Bida T., Zuckerman B., Becklin E. E., Chabrier G., Baraffe I., 1999, ApJ, 519, 834
Kirkpatrick J. D. et al., 2011, ApJS, 197, 19
Kraus A. L., Ireland M. J., Martinache F., Lloyd J. P., 2008, ApJ, 679, 762
Kraus A. L., Tucker R. A., Thompson M. I., Craine E. R., Hillenbrand L. A., 2011, ApJ, 728, 48
Latham D. W., Mazeh T., Stefanik R. P., Mayor M., Burki G., 1989, Nat, 339, 38
Liu M. C., Fischer D. A., Graham J. R., Lloyd J. P., Marcy G. W., Butler R. P., 2002, ApJ, 571, 519
Loeb A., Gaudi B. S., 2003, ApJ, 588, L117
Lovis C. et al., 2011, A&A, 528, 112
Lucy L. B., 1967, ZA, 65, 89
Madhusudhan N., Burrows A., 2012, ApJ, 747, 25
Mazeh T., Nachmani G., Sokol G., Faigler S., Zucker S., 2012, A&A, 541, 56
Morris S. L., Naftilan S. A., 1993, ApJ, 419, 344
Pfahl E., Arras P., Paxton B., 2008, ApJ, 679, 783
Prsa A. et al., 2011, AJ, 141, 83
Reffert S., Quirrenbach A., 2011, A&A, 527, 140
Ribas I., 2006, Ap&SS, 304, 89
Ricker G. R. et al., 2010, AAS Meeting 215, BAAS, 42, 459
Saffe C., Gómez M., Chavero C., 2005, A&A, 443, 609
Saumon D., Geballe T. R., Leggett S. K., Marley M. S., Freedman R. S., Lodders K., Fegley B., Sengupta S. K., 2000, ApJ, 541, 374
Scholz A., Irwin J., Bouvier J., Sipőcz B. M., Hodgkin S., Eislöffel J., 2011, MNRAS, 413, 2595
Seager S., Whitney B. A., Sasselov D. D., 2000, ApJ, 540, 504
Seager S., Kuchner M., Hier-Majumder C. A., Militzer B., 2007, ApJ, 669, 1279
Selsis F., Wordsworth R. D., Forget F., 2011, A&A, 532, 1
Sengupta S., Krishan V., 2000, A&A, 358, L33
Showman A. P., Fortney J. J., Lian Y., Marley M. S., Freedman R. S., Knutson H. A., Charbonneau D., 2009, ApJ, 699, 564
Shporer A. et al., 2011, AJ, 142, 195
Simpson E. K., Baliunas S. L., Henry G. W., Watson C. A., 2010, MNRAS, 408, 1666
Smalley B., 2005, Mem. Soc. Astron. Ital. Suppl., 8, 130
Soszyński I. et al., 2004, Acta Astron., 54, 347
Sozzetti A., Casertano S., Lattanzi M. G., Spagna A., 2001, A&A, 373, L21
Spiegel D. S., Burrows A., Milsom J. A., 2011, ApJ, 727, 57
Sudarsky D., Burrows A., Hubeny I., Li A., 2005, ApJ, 627, 520
Takeda G., Ford E. B., Sills A., Rasio F. A., Fischer D. A., Valenti J. A., 2007, ApJS, 168, 297
Torres G., Andersen J., Giménez A., 2010, A&AR, 18, 67
Udry S., Mayor M., Naef D., Pepe F., Queloz D., Santos N. C., Burnet M., 2002, A&A, 390, 267
Valenti J. A., Fischer D. A., 2005, ApJS, 159, 141
van Kerkwijk M. H., Rappaport S. A., Breton R. P., Justham S., Podsiadlowski P., Han Z., 2010, ApJ, 715, 51
Watson C. A., Littlefair S. P., Collier Cameron A., Dhillon V. S., Simpson E. K., 2010, MNRAS, 408, 1606
Welsh W. F., Orosz J. A., Seager S., Fortney J. J., Jenkins J., Rowe J. F., Koch D., Borucki W. J., 2010, ApJ, 713, L145
Wilsey N. J., Beaky M. M., 2009, SASS, 28, 107
Wilson R. E., 1990, ApJ, 356, 613
Winn J. N. et al., 2005, ApJ, 631, 1215
Zaqarashvili T., Javakhishvili G., Belvedere G., 2002, ApJ, 579, 810
Zucker S., Mazeh T., Alexander T., 2007, ApJ, 670, 1326

This paper has been typeset from a TEX/LATEX file prepared by the author.

Downloaded from http://mnras.oxfordjournals.org/ at California Institute of Technology on April 13, 2016